JACS
JOURNAL OF THE AMERICAN CHEMICAL SOCIETY
Article
pubs.acs.org/JACS

# Enhancing the Reversibility of Mg/S Battery Chemistry through $Li^+$ Mediation

Tao Gao,[†,⊥] Malachi Noked,[*,‡,§,⊥] Alex J Pearse,[‡] Eleanor Gillette,[§] Xiulin Fan,[†] Yujie Zhu,[†] Chao Luo,[†] Liumin Suo,[†] Marshall A Schroeder,[‡] Kang Xu,[∥] Sang Bok Lee,[*,§] Gary W. Rubloff,[*,‡] and Chunsheng Wang[*,†]

[†]Department of Chemical and Biomolecular Engineering, [‡]Department of Material Science and Engineering, and [§]Department of Chemistry and Biochemistry, University of Maryland, College Park, College Park, Maryland 20740, United States

[∥]Electrochemistry Branch, Power and Energy Division Sensor and Electron Devices Directorate, U.S. Army Research Laboratory, Adelphi, Maryland 20783, United States

Supporting Information

**ABSTRACT:** Mg metal is a promising anode material for next generation rechargeable battery due to its dendrite-free deposition and high capacity. However, the best cathode for rechargeable Mg battery was based on high molecular weight $Mg_xMo_3S_4$, thus rendering full cell energetically uncompetitive. To increase energy density, high capacity cathode material like sulfur is proposed. However, to date, only limited work has been reported on Mg/S system, all plagued by poor reversibility attributed to the formation of electrochemically inactive $MgS_x$ species. Here, we report a new strategy, based on the effect of $Li^+$ in activating $MgS_x$ species, to conjugate a dendrite-free Mg anode with a reversible polysulfide cathode and present a truly reversible Mg/S battery with capacity up to 1000 mAh/$g_s$ for more than 30 cycles. Mechanistic insights supported by spectroscopic and microscopic characterization strongly suggest that the reversibility arises from chemical reactivation of $MgS_x$ by $Li^+$.

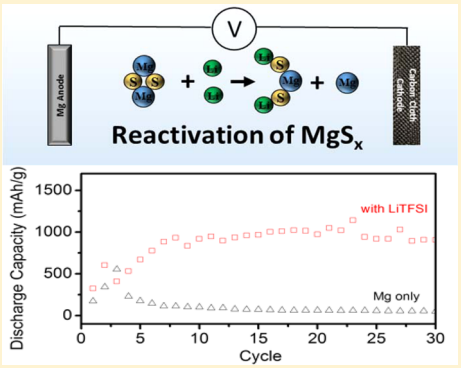


## INTRODUCTION

Rechargeable magnesium chemistry has long been considered a potential candidate for beyond Li-ion batteries (LIB) due to several unique properties. Magnesium metal has a rather negative potential (−2.36 V vs NHE), high abundance in earth-crust and less reactivity toward moisture and air. More importantly, magnesium metal can be directly used as anode material in an ethereal magnesium organohaloaluminate electrolyte with close to 100% deposition/stripping efficiency without forming undesirable dendrites, providing a high capacity of 2205 mAh/g and 3833 mAh/cc.[1] However, the sluggish intercalation kinetics of $Mg^{2+}$ into host structures originated from its bivalency[2,3] and the narrow electrochemical stability window of Mg battery electrolytes (<3.5 V)[4−10] have severely restricted the choice of rechargeable magnesium battery (RMB) cathodes,[11−14] enabling only limited energy densities for the full RMB system. Progress in Mg compatible electrolytes that allow the use of high voltage cathodes, and development of reversible high capacity cathodes are critical for the success of RMBs. As a high capacity cathode material (1675 mAh/g), sulfur has attracted intense interest in Li−S and Na−S systems.[15−20] Because the reduction of sulfur in the presence of cations ($Li^+$, $Na^+$ or $Mg^{2+}$) is nontopotactic and does not depend on solid-state ion transport, use of sulfur cathodes could presumably yield a fast cathode reaction for RMBs. Realization of a Mg/S battery is also of great interest because the full cell theoretical capacity could achieve up to 957 mAh/(g-total electrode mass) with an average voltage of 1.77 V as estimated based on the Gibbs formation energy of magnesium sulfide, −341.8 kJ/mol.[21] The theoretical specific energy is hence 1722 Wh/kg, over four times that of a commercial $LiCoO_2$/graphite cell and close to that of a $Li_2S$/silicon cell (Table S1), making it an exceptionally promising battery chemistry for large-scale (103−106 Wh) applications like electric vehicle and grid storage that require both high energy density and low cost.

Unfortunately, the magnesium organohaloaluminate electrolyte that allows reversible Mg deposition is synthesized by in situ reaction between Lewis acid ($AlCl_3$) and nucleophilic Lewis base (RMgCl), which reacts with the electrophilic sulfur cathode.[6] To circumvent this incompatibility, Kim et al. proposed a new electrolyte system using non-nucleophilic hexamethyldisilazide magnesium chloride (HMDSMgCl), and reported the first proof-of-concept Mg/S battery.[22] This electrochemical couple operates at a very low potential (0.89 V), and loses ∼70% capacity at the second discharge. More recently, Zhao-Karger et al. developed a novel non-nucleophilic electrolyte based on magnesium-bis(hexamethyldisilazide) [$(HMDS)_2Mg$] using various ether solvents and ionic liquid

**Received:** July 31, 2015
**Published:** September 11, 2015





DOI: 10.1021/jacs.5b07820
J. Am. Chem. Soc. 2015, 137, 12388−12393

additives, and investigated the reaction mechanism of a Mg/S cell by XPS.[23] However, despite the two discharge plateaus at 1.5 and 0.7 V during initial sulfur reduction, no plateau was observed in the following cycles. Indeed, the capacity dropped more than 60% after the second cycle. In summary, so far, no real reversible Mg/S battery has been demonstrated, primarily due to the electrochemical inactivity of the formed lower order Mg polysulfides (Mg-PS) toward oxidation.[23]

We introduce herein a new strategy to enhance the reversibility of Mg/S chemistry. A non-nucleophilic Mg electrolytes with LiTFSI additive enables the conjugation of reversible polysulfide redox reaction on cathode with Mg deposition/stripping on anode. Reversible discharging/charging of the Mg/S cell is demonstrated for over 30 cycles with specific cathode capacity comparable to the sister Li/S system. Two possible mechanisms for the enhanced reversibility are suggested: (1) $Li^+$ participates in the cathode reaction to form readily rechargeable Li polysulfide (Li-PS) or incorporates into Mg-PS to form hybrid Mg/Li polysulfide (MgLi-PS) during discharge, or (2) the hard Lewis acid $Li^+$ strongly coordinates to the surface $S^{2-}$ of lower order Mg-PS, hence enhancing its solubility, decreasing its reoxidation energy barrier and making it electrochemically active. The first role can be deduced from the facts that the cathode redox couple in a RMB can be tailored by changing the relative activity of $Mg^{2+}$ and $Li^+$,[24−29] and that crystalline MgS starts to lithiate in Li electrolyte when potential decreases to 1.7 V vs $Li/Li^+$ (1 V vs $Mg/Mg^{2+}$).[30] On the other hand, the positive effect of Lewis acids on the reversibility of sulfides is well-known, which provides strong supports for the second role of $Li^+$.[31] Though further studies are needed to realize a practical Mg/S system, specifically in terms of electrolyte volume and Li salt concentrations, we strongly believe that system optimization based on the new scientific insights obtained in this work will pave the path for the realization of practical rechargeable Mg/S battery.

## EXPERIMENTAL METHODS

**Electrolyte Preparation.** Electrolytes were prepared under pure argon atmosphere in VAC, Inc. glovebox (<1 ppm of water and oxygen). The non-nucleophilic Mg electrolyte based on $(HMDS)_2Mg$ (denoted as Mg-HMDS) was synthesized following previously reported procedure.[23] The electrolyte was prepared by adding lithium bis(trifluoromethanesulfonyl)imide (LiTFSI) into the non-nucleophilic $(HMDS)_2Mg$-based electrolytes (denoted as Mg-HMDS) and stirring overnight. The LiTFSI salt was baked at 80 °C in glovebox overnight before use.

**Battery Fabrication.** ACC/sulfur cathode was made following previous procedure.[32] Typical sulfur loading is 0.5 $mg/cm^2$ in this study. The thickness of the ACC is ~0.47 mm. Mg foil was used as anode and Whatman Glass fiber as separator.

**Electrochemical Measurement.** Galvanostatic tests were carried out in Swagelok cell with Arbin Instrument. Inconel alloy rod was used as current collector, due to its electrochemical stability against the electrolyte.[33] Cyclic voltammetry of the electrolytes was performed in a three-electrode cell with Pt disk as working and Mg foil as both counter and reference electrodes on Gamry Reference 3000.

**Material Characterization.** The morphology of the deposition in the dual-ion electrolyte and the morphology of ACC/S cathode were examined using a Hitachi SU-70 field-emission scanning electron microscope. X-ray powder diffraction patterns were obtained on Bruker Smart 1000 (Bruker AXS, Inc.) using Cu K$\alpha$ radiation with an airtight holder from Bruker. Raman measurements were performed on a Horiba Jobin Yvon Labram Aramis using a 532 nm diode-pumped solid-state laser, attenuated to give 900 mW power at the sample surface. FT-IR tests were performed on a Thermo Nicolet NEXUS 670. XPS analysis was measured with a Kratos AXIS Ultra DLD instrument using monochromated Al K$\alpha$ X-rays as the excitation source. For ICP measurements, 400 $\mu$L of TEGDME from each corrosion test was evaporated and the remaining solids were diluted in 3% $HNO_3$ solution (4.125 mL). ICP-OES measurements were performed using a Shimadzu ICPE-9820 Dual View Spectrometer. Intensities were measured at 280.270 nm for Mg and calibration curves were made from Mg standards (Sigma-Aldrich), traceable to the National Institute of Standards and Technology (NIST).

## RESULTS AND DISCUSSION

The Mg deposition/stripping in electrolytes with and without LiTFSI was characterized by cyclic voltammetry in a three-electrode cell using a platinum disk as the working electrode and Mg foil as both counter and reference electrodes (Figure 1). As illustrated, the overpotential for Mg deposition is −0.5 V

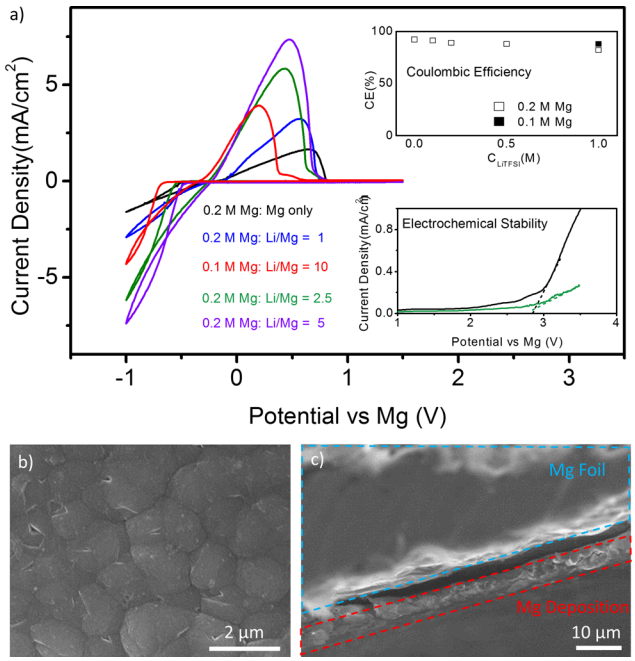


**Figure 1.** (a) Cyclic voltammograms of Mg deposition/stripping in a three-electrode cell at a scan rate of 100 mV/s at room temperature. Inset: Coulombic efficiency of Mg deposition/stripping and electrochemical stability of the electrolyte. The onset of electrolyte decomposing can be identified through the intersection of *x*-axis with the tangent of current rise at the end of anodic scan (dashed line). (b) Top view and (c) cross-section of Mg deposition on Mg foil in 0.1 M Mg-HMDS + 1.0 M LiTFSI electrolyte.

for 0.2 M Mg-HMDS and does not change significantly with increased Li concentration. The Coulombic efficiencies are calculated based on the ratio of dissolved Mg to deposited Mg (Figure 1 inset). Efficiency of 92% is observed for Mg-HMDS with slight decrease upon addition of Li salt. The anodic stability of the electrolyte is given in Figure 1 inset. As shown, the onset of electrolyte decomposing is slightly decreased to ~2.7 V upon $Li^+$ addition. The deposition/dissolution current density rises with increasing Li concentration due to higher ionic conductivity of the electrolyte, similar to what has been demonstrated by Gofer et al.[34] Reducing Mg concentration from 0.2 to 0.1 M suppresses the current response but slightly improves the Coulombic efficiency.

Since the most important merit of Mg anode is its dendrite-free deposition in ethereal Mg organohaloaluminate electrolytes,[4,35,36] it is important to examine the influence of large


DOI: 10.1021/jacs.5b07820
J. Am. Chem. Soc. 2015, 137, 12388−12393

overpotential and high current density on the morphology of deposits in the electrolyte with LiTFSI additive. Thus, we held Mg foil at −1.2 V vs Mg RE (current density ∼1 mA/cm$^2$) for 1 h in 0.1 M Mg-HMDS + 1.0 M LiTFSI electrolyte, and conducted microscopic studies on the deposits. Scanning electron microscopy (SEM) images show that the deposits are initially spheres of diameters ∼2 μm, and as they grow bigger, they squeeze each other and deform into tightly packed polygons (Figure 1b and Figure S1). The cross-sectional image shows no observable dendrite formation (Figure 2c). These results prove that the deposits have uniform two-dimensional morphology similar to the deposition in Mg-only electrolyte.[4,35,36]

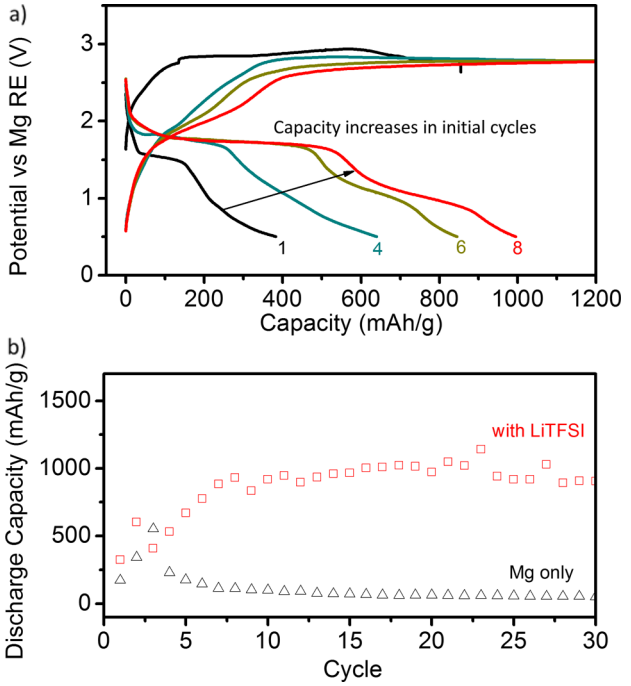


**Figure 2.** (a) Charge/discharge curves of sulfur cathode in 0.1 M Mg-HMDS + 1.0 M LiTFSI electrolyte in a three electrode cell at a current of 71 mAh/g at room temperature. Arrow illustrates the capacity increasing trend of the ACC/S composite cathode as a result of slow electrolyte penetration.[16] (b) Cycling stability of the Mg/S battery in electrolyte with and without LiTFSI.

Although it is thermodynamically unlikely for Li deposition to appear on Mg anode in the dual-ion electrolyte since the standard reduction potential of Li (−3.04 V vs NHE) is 0.68 V lower than that of Mg (−2.36 V vs NHE), large overpotential may lower the potential of the Mg anode sufficiently for Li deposition or Li−Mg alloying. However, powder X-ray Diffraction (XRD) of the deposits excluded such possibilities by showing only metallic Mg and no detectable Li metal, Li−Mg alloy or other Li compound (Figure S2). X-ray photoelectron spectroscopy (XPS) data were also collected (Figure S3), and atomic quantification of the deposit strongly suggests that only Mg is electrodeposited under these conditions (see Supporting Information for further discussion). In summary, the addition of a relatively high concentration of $Li^+$ does not negatively impact the Mg deposition/stripping and its morphology, and only Mg is active at the relevant potentials. These observations, consistent with our previous work,[24] suggest that this electrolyte can be used in a RMB without causing detectable Li deposition/alloying and dendrite formation.

We next fabricated full cells with Mg anodes and sulfur cathodes in the electrolytes. SEM images and element analysis by energy dispersive X-ray spectroscopy (EDS) of the ACC/S composite cathode are presented in Figure S4a. The fibers in ACC/S cathodes are clearly observed. The element mapping shows that sulfur is uniformly dispersed inside the fiber. Thermogravimetric analysis (TGA) in Figure S4b shows that sulfur content is 15% in the composite. XRD pattern of ACC/S cathode is presented in Figure S4c. Two broad diffraction peaks around 2$\theta$ of 24° and 44° correspond to (002) and (100)/(101) planes of graphite, suggesting the existence of small domains of ordered graphene sheets in ACC. The absence of sulfur peaks indicates that sulfur is in a highly dispersed state inside the pores, in agreement with previous report.[16]

The ACC/S cathode was closed in a custom-built three-electrode cell with Mg foil as both counter and reference electrodes. Typical charge−discharge voltage profiles measured during galvanostatic cycling in 0.1 M Mg-HMDS + 1.0 M LiTFSI electrolyte are presented in Figure 2a. The capacity increases in initial cycles, a typical behavior of ACC/S cathodes in Li/S cells due to slow penetration of electrolyte into the pores inside carbon.[16,32] During this infiltration process, sulfur utilization gradually increases with cycling,[6] and reaches its maximum at the eighth cycle. Continued cycling yields a stable capacity of roughly 1000 mAh/$g_s$. The eighth discharge voltage profile (Figure 2a) contains two plateaus, the first of which (∼550 mAh/$g_s$) is observed at ∼1.75 V, followed by a slope leading to the second plateau at ∼1.2 V(∼300 mAh/$g_s$). The two reduction plateaus are in good agreement with those reported in Zhao-Karger's work, indicating the formation of high-order and low-order polysulifides, respectively.[23] However, since Li-PS redox reaction takes place at similar potentials,[15,29] it is likely that Li-PS also forms simultaneously. MgLi-PS may also form due to $Li^+$ incorporating into Mg-PS at this potential domain.[30] However, despite $Li^+$ possibly involves in sulfur reduction, the discharge pathway is more likely dominated by Mg-PS instead of Li-PS, since Li-PS reduction as reported in literature shows a short plateau of ∼250 mAh/$g_s$ followed by a long plateau of ∼700 mAh/$g_s$ for ACC/sulfur cathode,[30] which is distinctly different from the voltage profile presented in Figure 2a, in which the first plateau is longer (∼550 vs typical 250 mAh/$g_s$ for Li/S systems) and the second plateau at the lower voltage is shorter (∼300 vs 700 mAh/$g_s$). Two plateaus are observed in the recharge process as well, the first of which at ∼1.8 V corresponds to the oxidation of low order PS. This plateau is seldom seen in previous Mg/S cell,[23] thus its appearance suggests enhanced electrochemical activity of short chain PS in the presence of $Li^+$. The second plateau at ∼2.7 V arises from oxidation of the high order PS. Potential rise usually seen at the end of recharge plateau in Li/S cells[15,16] was not observed even at high rate (1C) in this work, possibly due to electrolyte decomposition or shuttle phenomena. For this reason, the recharge process presented in Figure 2a was conducted at a high rate (1C), and was immediately cut off when theoretical capacity is reached in order to minimize possible side reactions. Negligible overpotential was required for Mg dissolution and an initial overpotential of −0.55 V was needed to drive Mg deposition on Mg foil, but it drops gradually to −0.1 V during cycling (Figure S5). Since thermodynamically polysulfide should be reduced on the metallic Mg anode, shuttle effect should also exist in our


DOI: 10.1021/jacs.5b07820
J. Am. Chem. Soc. 2015, 137, 12388−12393

system, as supported by XPS of the anode (see the discussion below). Unfortunately, due to the cycling protocol used herein and due to the possible parasitic reactions like electrolyte decomposition, and because the capacity utilization of sulfur is not complete, we cannot link the apparent Coulombic efficiency to the extent of shuttle effect in our cell.

The cycling stability in electrolyte with and without LiTFSI additive is given in Figure 2b. Consistent with previous work,[23] sulfur cathode shows rapid capacity drop in Mg-only electrolyte, while $Li^+$ presence dramatically improves the reversibility of the cell, which retains a stable capacity of ~1000 mAh/$g_s$ for 30 cycles. The result strongly suggests that the presence of $Li^+$ dictates the reversibility of the cathode, as will be discussed more mechanistically bellow (see Scheme 1). To the best of our knowledge, this is the best reversibility achieved so far for a Mg/S system.

**Scheme 1. Working Mechanism of the Mg/S Battery with LiTFSI Additive**

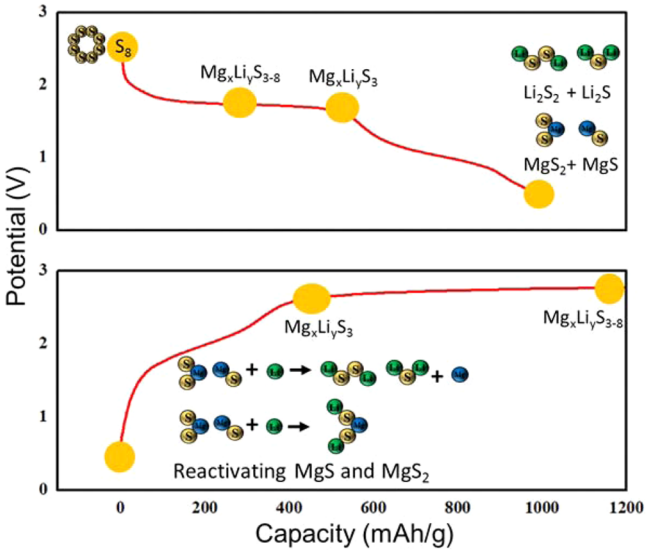


To identify the effect of $Li^+$ on the anode side, surface chemistry of Mg anodes recovered after cycling in electrolytes with and without LiTFSI were characterized using XPS. A comparison of the S 2p energy region reveals significant differences in the surface chemistry involving sulfur, as shown in Figure 3. The Mg anode surface always contains multiple chemical states of sulfur, fit with constrained spin−orbit split doublets. The anode recovered from Mg-only electrolyte, as shown in Figure 3a, has a surface layer composed of sulfur species that are either oxidized ($MgSO_4$ at ~169 eV and $MgSO_3$ at ~167 eV), elemental or slightly reduced (~163.5 eV), or highly reduced (MgS at ~161.5 eV).[37] MgS is an expected product, which forms from exposure to dissolved S species, due to the known shuttle mechanism, as also shown in Figure S6. When LiTFSI is added (Figure 3b), the surface chemistry changes dramatically, as shown in Figure 3b. The presence of residual chemisorbed TFSI anions on the surface leads to a dominant peak at 169 eV associated with the S(VI) atom in the anion. Because the overall count rate from each anode was very similar, Figure 3a,b is plotted with the same total *y*-scale (300 counts/s) to allow for a direct comparison of the non-TFSI components. There is an increase in $SO_3^{2-}$, due to a known TFSI decomposition product.[38] Most importantly,

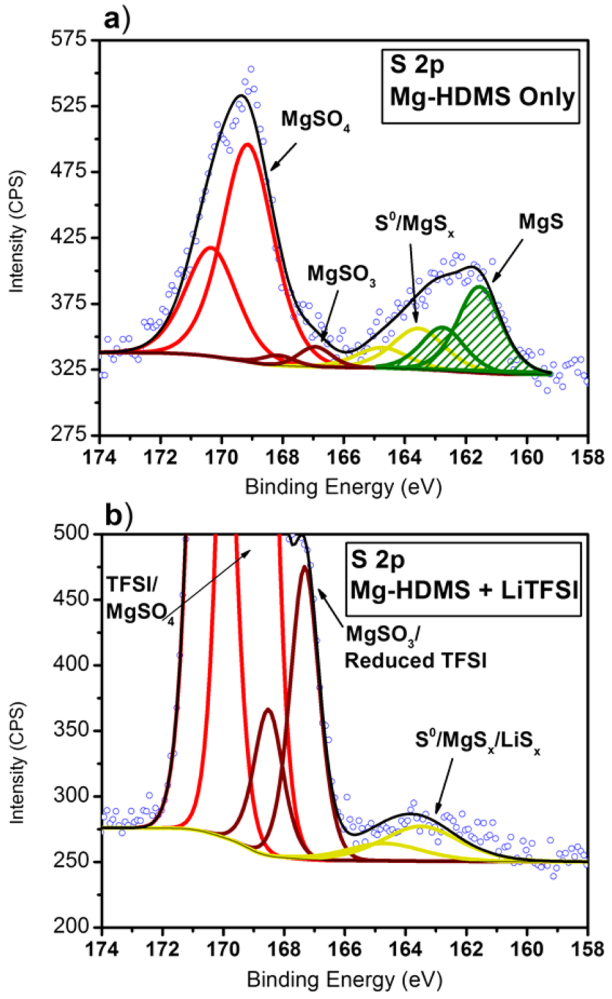


**Figure 3.** Comparison of surface XPS measurements of Mg anode cycled in Mg-HDMS in the absence (a) and presence (b) of LiTFSI.

the XPS spectra indicate the absence of MgS in electrolyte with LiTFSI additive. This directly supports the notion that the hard Lewis acid $Li^+$ plays an active role in dissolving MgS, either by coordinating to the surface $S^{2-}$ of MgS and increasing its solubility,[31] or by lithiating MgS due to the natural negative potential of Mg metal, forming soluble higher order MgLi-PS.[30]

To obtain more direct chemical proof for the role of $Li^+$ in the cathode, spectroscopic studies were conducted to identify possible species existing in the electrolyte of the discharged cell. However, we could not unambiguously distinguish between the two possible polysulfides involved (Mg-PS or Li-PS) by FTIR, Raman or XPS (Figure S7). XRD was also not capable of identifying the phases of discharged product since sulfur is in a highly dispersed state inside the pores.[16]

Thus, alternative experiment is designed to reveal the mechanism. Since the kinetics of the PS redox reaction is known to be highly dependent on the solubility of the reduced sulfur species,[31,39] and reoxidation of the inactive/insoluble short chain Mg-PS is reported to be the major limitation on reversibility of Mg/S battery,[23] we conducted a Mg metal corrosion experiment to explore the effect of $Li^+$ on the solubility of short chain Mg-PS species.

It is known that Li metal will be corroded by elemental sulfur in ethereal solvent, leading to the formation of soluble Li-PS with a yellow/brown color (Figure S8). The reaction in turn


DOI: 10.1021/jacs.5b07820
J. Am. Chem. Soc. 2015, 137, 12388−12393

increases sulfur solubility (as Li-PS) up to a few moles.[31] However, in our experiment, the visible corrosion of Mg under similar conditions never happen even after 3 weeks (Figure S9a). Though no clear appearance of PS is obtained in the liquid, the formation of an MgS layer on the Mg foil was detected by XPS (Figure S6). This surface layer protects the bulk of the Mg from further corrosion by sulfur, similar to the manner where natural layer of MgO passivate Mg from oxidation in ambient conditions. Interestingly, the addition of LiTFSI to Mg/S/TEGDME under the same condition turns TEGDME to yellow (typical for polysulfide in glymes) after only 12 h (Figure S9b) and to brown after 54 h (Figure S9c). This strongly suggests that the surface layer of MgS is dissolved by the action of $Li^+$ and Mg surface could not be passivated anymore, which is in excellent agreement with Figure 3 as discussed above. To confirm whether MgS is indeed dissolved, we used ICP-OES to examine the presence of dissolved Mg in TEGDME solution after the corrosion experiment. The concentration of Mg in the TEGDME was negligible when no $Li^+$ was present (<8 $\mu$g/L), indicating negligible presence of Mg-PS in TEGDME. However, the concentration of Mg increased by 3 orders of magnitude (>0.65 mg/L) in the presence of $Li^+$ after 12 h of LiTFSI addition. The corrosion of Mg continued (Figure S9c), increasing the concentration of Mg by another order of magnitude after 54 h (>8.4 mg/L). The result is consistent with our XPS observation on Mg foil in electrolyte with and without LiTFSI (Figure 3), and double confirms our hypothesis that the mediation role of $Li^+$ on the rechargeability of low order Mg-PS is originating from its effect on Mg-PS solubility: either hard Lewis acid ($Li^+$) strongly coordinates with the hard base surface $S^{2-}$ in the formed low order Mg-PS and assists its dissolution, or $Li^+$ is driving the solubility of surface MgS through ion exchange reaction (MgS to $Li_2S$). It is also possible that MgS is first lithiated by $Li^+$ due to the natural negative potential of the Mg metal and then the formed MgLi-PS enables further reaction with the dissolved elemental sulfur to form soluble higher order MgLi-PS.

Previous work on Mg/S system claims that sulfur reduction reaction takes place in two steps in ether solvents: a fast solid–liquid two phase reduction forming high order polysulfide ($MgS_8$, $MgS_6$, $MgS_4$), followed by a sluggish liquid–solid reduction forming insoluble $MgS_2$ and MgS.[23] The low order Mg-PS produced during the first discharge in Mg/S cell loses its electrochemical activity in the subsequent recharge due to high kinetic barriers originating from its insulating nature and insolubility.[23] However, as demonstrated in the corrosion experiment, the solubility of short chain Mg-PS increases dramatically due to assistance of $Li^+$, potentially lowering the kinetic barrier for reoxidation of Mg-PS. We therefore suggest that the reduction of sulfur in our battery occurs via the following sequences:

(1) Sulfur reduction starts by the formation of soluble long chain MgLi-PS. Since the first discharge plateau provides about one-third of sulfur's theoretical capacity (558 mAh/g), the formed product should have the stoichiometry of $MS_3$, M = $Mg_xLi_y$.

(2) Further reduction will lead to either reversible short chain Li-PS ($Li_2S$ and $Li_2S_2$), or short chain Mg-PS (MgS and $MgS_2$).

The oxidation of discharged product during recharge occurs via following steps:

(1) During charge, the short chain Li-PS ($Li_2S$ and $Li_2S_2$) will oxidize to form longer chain PS ($Li_2S_8$).

(2) The presence of $Li^+$ enables reactivation of the short chain Mg-PS (MgS and $MgS_2$) either through an ion echange reaction and transforms them into rechargeable $Li_2S$ and $Li_2S_2$,[30] or through strong coordination of $Li^+$ with the surface $S^{2-}$ and $S_2^{2-}$ of MgS and $MgS_2$ that increase their solubility and reduce the reoxidation kinetic barrier by forming MgLi-PS.[31] A schematic illustration of the proposed mechanism, and the correlated voltage profile, is presented in Scheme 1.

## CONCLUSION

We demonstrated a rechargeable Mg/S battery with much improved reversibility by using LiTFSI as additive. We show that our system combines the dendrite free deposition/striping of Mg anode with reversible redox reaction of sulfur cathode through activation of inactive MgS and $MgS_2$ by $Li^+$. The cell demonstrated a capacity of 1000 mAh/$g_s$ with two discharge plateaus at 1.75 and 1.0 V, corresponding to an obtainable energy density of 874 Wh/kg. It showed stable capacity up to 30 cycles. The assisting effect of $Li^+$ on Mg/S solubility in TEGDME, a key parameter controlling the reversibility of sulfur cathodes, is revealed by XPS on cycled Mg anode and confirmed by corrosion experiments. It is, to our knowledge, the first realization of a convincingly reversible Mg/S battery chemistry. Although the amount of electrolyte required is dictated by the required $Li^+$, necessitating an excess electrolyte volume, this work undoubtedly opens a new avenue that could lead to a fully rechargeable Mg/S system with further optimization, while shedding light on the mechanism of how $Li^+$ mediates the electrochemical reactions. More sophisticated cell designs, such as a polysulfide flow battery or use of a different Lewis acid can be applied in order to achieve a practical Mg/S battery based on our findings.

## ASSOCIATED CONTENT

### Supporting Information

The Supporting Information is available free of charge on the ACS Publications website at DOI: 10.1021/jacs.5b07820.

Additional experimental results (PDF)

## AUTHOR INFORMATION


### Corresponding Authors

*cwang@umd.edu
*rubloff@umd.edu
*slee@umd.edu
*mnoked@gmail.com

### Author Contributions

⊥T.G. and M.N. contributed equally.


### Notes

The authors declare no competing financial interest.

## ACKNOWLEDGMENTS

This work was supported as part of the Nanostructures for Electrical Energy Storage (NEES), an Energy Frontier Research Center funded by the U.S. Department of Energy, Office of Science, Basic Energy Sciences under Award Number DESC0001160. We acknowledge the support of the Maryland NanoCenter and its AIM Lab. We acknowledge the Environmental Engineering Lab for use of their ICP-OES. We acknowledge Professor Doron Aurbach, Dr. Kevin Leung and Mr. Fudong Han for their valuable comments.



DOI: 10.1021/jacs.5b07820
J. Am. Chem. Soc. 2015, 137, 12388–12393

## REFERENCES


(1) Yoo, H. D.; Shterenberg, I.; Gofer, Y.; Gershinsky, G.; Pour, N.; Aurbach, D. *Energy Environ. Sci.* **2013**, *6*, 2265.
(2) Levi, E.; Levi, M. D.; Chasid, O.; Aurbach, D. *J. Electroceram.* **2009**, *22*, 13.
(3) Levi, E.; Gofer, Y.; Aurbach, D. *Chem. Mater.* **2010**, *22*, 860.
(4) Mizrahi, O.; Amir, N.; Pollak, E.; Chusid, O.; Marks, V.; Gottlieb, H.; Larush, L.; Zinigrad, E.; Aurbach, D. *J. Electrochem. Soc.* **2008**, *155*, A103.
(5) Doe, R. E.; Han, R.; Hwang, J.; Gmitter, A. J.; Shterenberg, I.; Yoo, H. D.; Pour, N.; Aurbach, D. *Chem. Commun.* **2014**, *50*, 243.
(6) Liu, T.; Shao, Y.; Li, G.; Gu, M.; Hu, J.; Xu, S.; Nie, Z.; Chen, X.; Wang, C.; Liu, J. *J. Mater. Chem. A* **2014**, *2*, 3430.
(7) Zhao-Karger, Z.; Zhao, X.; Fuhr, O.; Fichtner, M. *RSC Adv.* **2013**, *3*, 16330.
(8) Carter, T. J.; Mohtadi, R.; Arthur, T. S.; Mizuno, F.; Zhang, R.; Shirai, S.; Kampf, J. W. *Angew. Chem., Int. Ed.* **2014**, *53*, 3173.
(9) Guo, Y.; Zhang, F.; Yang, J.; Wang, F.; NuLi, Y.; Hirano, S. *Energy Environ. Sci.* **2012**, *5*, 9100.
(10) Cheng, Y.; Stolley, R. M.; Han, K. S.; Shao, Y.; Arey, B.; Washton, N.; Mueller, K. T.; Helm, M. L.; Sprenkle, V. L.; Liu, J.; Li, G. *Phys. Chem. Chem. Phys.* **2015**, *17*, 13307.
(11) Aurbach, D.; Suresh, G. S.; Levi, E.; Mitelman, A.; Mizrahi, O.; Chusid, O.; Brunelli, M. *Adv. Mater.* **2007**, *19*, 4260.
(12) Liang, Y.; Feng, R.; Yang, S.; Ma, H.; Liang, J.; Chen, J. *Adv. Mater.* **2011**, *23*, 640.
(13) NuLi, Y.; Zheng, Y.; Wang, Y.; Yang, J.; Wang, J. *J. Mater. Chem.* **2011**, *21*, 12437.
(14) Liang, Y.; Yoo, H. D.; Li, Y.; Shuai, J.; Calderon, H.; Robles Hernandez, F. C.; Grabow, L. C.; Yao, Y. *Nano Lett.* **2015**, *15*, 2194.
(15) Ji, X.; Lee, K. T.; Nazar, L. F. *Nat. Mater.* **2009**, *8*, 500.
(16) Elazari, R.; Salitra, G.; Garsuch, A.; Panchenko, A.; Aurbach, D. *Adv. Mater.* **2011**, *23*, 5641.
(17) Mikhaylik, Y. V.; Akridge, J. R. *J. Electrochem. Soc.* **2004**, *151*, A1969.
(18) Liang, C.; Dudney, N. J.; Howe, J. Y. *Chem. Mater.* **2009**, *21*, 4724.
(19) Ji, L.; Rao, M.; Zheng, H.; Zhang, L.; Li, O. Y.; Duan, W. *J. Am. Chem. Soc.* **2011**, *133*, 18522.
(20) Jayaprakash, N.; Shen, J.; Moganty, S. S.; Corona, A.; Archer, L. A. *Angew. Chem., Int. Ed.* **2011**, *50*, 5904.
(21) Haynes, W. M. *CRC Handbook of Chemistry and Physics*; CRC Press: Boca Raton, FL, 2014.
(22) Kim, H. S.; Arthur, T. S.; Allred, G. D.; Zajicek, J.; Newman, J. G.; Rodnyansky, A. E.; Oliver, A. G.; Boggess, W. C.; Muldoon, J. *Nat. Commun.* **2011**, *2*, 427.
(23) Zhao-Karger, Z.; Zhao, X.; Wang, D.; Diemant, T.; Behm, R. J.; Fichtner, M. *Adv. Energy Mater.* **2015**, *5*, 140155.
(24) Gao, T.; Han, F.; Zhu, Y.; Suo, L.; Luo, C.; Xu, K.; Wang, C. *Adv. Energy Mater.* **2015**, *5*, 1401507.
(25) Yoo, H. D.; Liang, Y.; Li, Y.; Yao, Y. *ACS Appl. Mater. Interfaces* **2015**, *7*, 7001.
(26) Cho, J.; Aykol, M.; Kim, S.; Ha, J.; Wolverton, C.; Chung, K. Y.; Kim, K.; Cho, B. *J. Am. Chem. Soc.* **2014**, *136*, 16116.
(27) Cheng, Y.; Shao, Y.; Zhang, J. G.; Sprenkle, V. L.; Liu, J.; Li, G. *Chem. Commun.* **2014**, *50*, 9644.
(28) Yagi, S.; Ichitsubo, T.; Shirai, Y.; Yanai, S.; Doi, T.; Murase, K.; Matsubara, E. *J. Mater. Chem. A* **2014**, *2*, 1144.
(29) Wu, N.; Yang, Z. Z.; Yao, H. R.; Yin, Y. X.; Gu, L.; Guo, Y.-G. *Angew. Chem., Int. Ed.* **2015**, *54*, 5757.
(30) Wang, M.; Li, X.; Gao, M.; Pan, H.; Liu, Y. *J. Alloys Compd.* **2014**, *603*, 158.
(31) Rauh, R. D.; Abraham, K. M.; Pearson, G. F.; Surprenant, J. K.; Brummer, S. B.; Corporation, E. I. C. *J. Electrochem. Soc.* **1979**, *126*, 523.
(32) Kozen, A. C.; Lin, C.-F.; Pearse, A. J.; Schroeder, M. A.; Han, X.; Hu, L.; Lee, S.-B.; Rubloff, G. W.; Noked, M. *ACS Nano* **2015**, *9*, 5884.
(33) Wall, C.; Zhao-Karger, Z.; Fichtner, M. *ECS Electrochem. Lett.* **2015**, *4*, C8.
(34) Gofer, Y.; Chusid, O.; Gizbar, H.; Viestfrid, Y.; Gottlieb, H. E.; Marks, V.; Aurbach, D. *Electrochem. Solid-State Lett.* **2006**, *9*, A257.
(35) Aurbach, D.; Cohen, Y.; Moshkovich, M. *Electrochem. Solid-State Lett.* **2001**, *4*, A113.
(36) Matsui, M. *J. Power Sources* **2011**, *196*, 7048.
(37) Allison, D. a.; Johansson, G.; Allan, C. J.; Gelius, U.; Siegbahn, H.; Allison, J.; Siegbahn, K. *J. Electron Spectrosc. Relat. Phenom.* **1972**, *1*, 269.
(38) Aurbach, D.; Pollak, E.; Elazari, R.; Salitra, G.; Kelley, C. S.; Affinito, J. *J. Electrochem. Soc.* **2009**, *156*, A694.
(39) Cuisinier, M.; Cabelguen, P.-E.; Adams, B. D.; Garsuch, a.; Balasubramanian, M.; Nazar, L. F. *Energy Environ. Sci.* **2014**, *7*, 2697.




DOI: 10.1021/jacs.5b07820
*J. Am. Chem. Soc.* 2015, 137, 12388−12393